[UCI]I804:24011-200000285622

2020년 2월

박사학위 논문

Optical Characterization of Matallole Nanoaggregates and Their Sensing Applications

조 선 대 학 교 대 학 원

화 학 과

신 보 미 나

Optical Characterization of Matallole Nanoaggregates and Their Sensing Applications

메탈올 나노 응집체의 광학적 특성 분석 및 폭발물 센서 응용

2020년 2월 25일

조선대학교 대학원

화학과

신 보 미 나

Optical Characterization of Matallole Nanoaggregates and Their Sensing Applications

지도교수 손 홍 래

이 논문을 이학박사학위 신청 논문으로 제출함

2020년 10월

조선대학교 대학원

화학과

신 보 미 나

신보미나의 박사학위논문을 인준함

위원장	조선대학교	교수	이 범 규 (인)
위 원	조선대학교	교수	고 문 주 (인)
위 원	조선대학교	교수	손 홍 래 (인)
위 원	조선대학교	교수	김 호 중 (인)
위 원	세한대학교	교수	고 영 춘 (인)

2020년 12월

조선대학교 대학원

TABLE OF CONTENTS

TABLE OF CONTENTS i
LIST OF SYMBOLS AND ABBREVIATIONS iii
LIST OF FIGURES iv
ABSTRACT vii

PART 1
Optical Characterization of Dimethylsilole Nanoaggregates and Its Explosive Sensing Application 1

1.1. Introduction 1

1.2 Experiments 3

1.3. Results and Discussion 4

1.4. Conclusions 10

1.5. References 10

PART 2
Heavy Atom Effect on Metallole Nanoaggregates and Their Explosive Sensing Applications 13

2.1 Introduction 13

2.2 Experimental Details 14
2.2.1. General 15
2.2.2. Synthesis of Dimethyltetraphenylgermole(Germole) and Dimethyltetraphenylstannole(Stannole) 15
2.2.3. Instrumentation and Data Acquisition 16

2.3. Results and Discussion 17
2.3.1. Photophysical Propertis of Metalloles 17
2.3.2. Amplified Phtoluminescence of Metallole Nanoaggregates 17

2.3.3. Photoluminescence Quenching Studies with TNT..... 22

2.4. Conclusions..... 24

2.5. References..... 24

PART 3

TNT Sensor Based on Silole Nanoaggregates 27

3.1 Introduction..... 27

3.2 Experimental Details..... 29
3.2.1 General..... 29
3.2.2 Preparation of bis(methyltetraphenyl)silole..... 29
3.2.3 Preparation of bis(methyltetraphenyl)silole siloxane..... 29
3.2.4 Instruments and Data Acquisitions..... 30

3.3 Results and Discussion..... 30

3.4 Conclusions..... 37

3.5 References and Notes..... 37

LIST OF SYMBOLS AND ABBREVIATIONS

TNT	Trinitrotoluene
RDX	1,3,5-Trinitroperhydro-1,3,5-triazine
PETN	Pentaerythritol tetranitrate
DMDNB	2,3-dimethyl-2,3-dinitrobutane
lex	Exitation Wavelength
lem	Emission Wavelength
QY	Quantum Yield
DNT	Dinitrotoluene
PA	Picric Acid
π	Pi
δ	Delta
mg	Milligram
A.U.	Arbitrary Units
ppm	Part per Million
PL	Photoluminescence
nm	Nanometer
UV-Vis	Ultraviolet-Visible
M	Molarity
THF	Tetrahydrofuran
EA	Diethyl Ether
MC	Methylene Chloride

LIST OF FIGURES

PART 1
Optical Characterization of Dimethylsilole Nanoaggregates and Its Explosive Sensing Application

Figure 1.1 Optical Characterization of Dimethylsilole Nanoaggregates and Its Explosive Sensing Application

Figure 1.2 PL spectra of dimethylsilole molecule without aggregation and its nanoaggregate (a). PL spectra of dimethylsilole nanoaggregate in water-THF mixtures (% water from top; 90%, 80%, 70%, 60%, 50%, 40%, 30%, 20%, 10%, 0%) (b). Plot of the relative intensity of dimethylsilole nanoaggregate vs % water by volume and their photograph (c and d).

Figure 1.3 DLS data showing an increase in size when the water fraction ratio decreases to 90% (a) and 80% (b).

Figure 1.4 Quenching PL spectra of increasing fraction by 500 part per billion (ppb) of each TNT concentration in dimethylsilole nanoaggregates solution (a) and Stern-Volmer plot showing sensing efficiency for dimethylsilole nanoaggregate (b).

PART 2
Heavy Atom Effect on Metallole Nanoaggregates and Their Explosive Sensing Applications

Figure 2.1 UV-vis absorption spectra (solid line) and fluorescence spectra in THF in (dotted line) for (A) dimethyltetrapnenylgermole and

(B) dimethyltetraphenylstannole.

Figure 2.2 PL spectra of germole (A) and stannole (B) nanoaggregates in water-THF mixtures (99%, 90%, 80%, 70%, 60%, 50%, 40%, 30%, 20%, 10%, 0%). Plot of the relative intensity of germole nanoaggregate (red) and stannole nanoaggregate (blue) versus % water by volume (C).

Figure 2.3 DLS data showing an average particle diameter at the water fraction ratio of 99%, 90%, and 80% for germole nanoaggregates (A) and stannole nanoaggregates (B).

Figure 2.4 Quenching PL spectra upon addition of 500 part per billion (ppb) of each TNT for germole nanoaggregates (A) and stannole nanoaggregates (B). Stern-Volmer plot showing sensing efficiency for both nanoaggregates (C).

PART 3
TNT Sensor Based on Silole Nanoaggregates

Figure 3.1 Chemical structure of bis(methyltetraphenyl)silole (left) and bis(methyltetraphenyl)silole siloxane (right).

Figure 3.2 Schematic diagram for the preparation of silole nanoaggregates.

Figure 3.3 PL spectra of bis(methyltetraphenyl)silole (A) and bis(methyltetraphenyl)silole siloxane (B) nanoaggregates in water-THF mixtures (% water from top; 90%, 80%, 70%, 60%, 50%, 40%, 30%, 20%, 10%, 0%). Plot of the relative intensity of bis(methyltetraphenyl)silole nanoaggregate (red) and bis(methyltetraphenyl)silole siloxane nanoaggregate (blue) vs %

water by volume (C).

Figure 3.4 PL spectra of bis(methyltetraphenyl)silole (A) and bis(methyltetraphenyl)silole siloxane (B) nanoaggregates in water-THF mixtures (% water from top; 90%, 80%, 70%, 60%, 50%, 40%, 30%, 20%, 10%, 0%). Plot of the relative intensity of bis(methyltetraphenyl)silole nanoaggregate (red) and bis(methyltetraphenyl)silole siloxane nanoaggregate (blue) vs % water by volume (C).

Figure 3.5 Quenching PL spectra of increasing fraction by 500 part per billion (ppb) of each TNT concentration in bis(methyltetraphenyl)silole nanoaggregates solution (A) and bis(methyltetraphenyl)silole siloxane nanoaggregates solution (B). Stern-Volmer plot showing sensing efficiency for both nanoaggregates (C).

초 록

메탈올 나노응집체의 광학적 특성 분석 및 폭발물 센서 응용

박사과정 : 신 보 미 나
지도교수 : 손 홍 래
조선대학교 화학과

메탈올은 불포화 5각 고리에 실리콘이나 게르마늄 주석으로 치환된 화합물로서 최근에 그 독특한 광학적, 전자적 특성 때문에 유기전자 재료로서 흥미의 대상이 되어왔다. 이러한 독특한 성질들은 특히 광전자 기기에서 전자전달재료나 정공전달재료, 발광재료, 또는 화학적, 생물학적 센서에 매우 유용함. 최근 유기 발광재료들의 발광효율을 증가시키기 위한 연구는 매우 흥미의 대상이 되고 있는데 그 이유는 O-LED나 센서로서 응용할 경우 매우 중요하기 때문이다. 그러나 높은 발광성을 갖는 유기물이나 고분자는 고체 상태에서 덜 발광성을 갖는 종인 엑시머의 형성으로 인한 분자의 응집으로 발광성의 감소를 일으켰다. 최근에 발광성 유기분자가 응집된 고체 상태에서 발광효율이 증가하는 응집에 의해 유도되는 광 증폭효과의 특성을 갖는 분자가 흥미의 대상이 되고 있으나 여기에 관계된 보고는 소수에 불과하다. 본 연구는 메타올을 이용하여 응집 상태의 메탈올이 나노 크기 광 증폭 효과를 가진 특성이 있음을 선행연구에서 확인하고 더 나아가 메탈올의 원소 교환 효과 실리콘과 실리콘으로 연결되어 있는 시그마 시그마스타 효과 실리콘 사이

를 산소로 묶는 묶음 효과에 대해 현상에 대한 연구를 필요 하다고 사료된다.

한반도를 비롯한 전 세계 64개국에 모두 1억1천만 개 이상의 대인지뢰가 설치돼 인간의 생명을 위협하고 있다고 국제적십자위원회가 밝혔음. 현재 많은 선진국에서는 고감도 고성능 폭발물 탐지기를 개발하기 위해 나노소재, 전자코 어레이, nanoelectromechanical(NEME) 소자 등을 이용한 멀티모드 플랫폼 적용이 가능한 나노센서 등에 대한 연구가 이뤄져 오고 있다.

따라서 초극미량의 폭발물에도 고감도 고성능으로 탐지할 수 있는 새로운 센서의 개발은 자국 방위보안 시스템에서 필수적인 분야이며 세계적인 요구 사항으로 본 연구에서는 메탈올의 나노 크기 응집체를 통한 광 증폭효과로 인해 높아진 발광효율을 이용하여 초극미량에도 측정이 가능한 폭발물 탐지 연구를 진행하였다.

PART 1

Optical Characterization of Dimethylsilole Nanoaggregates and Its Explosive Sensing Application

1.1. Introduction

Highly emissive semiconducting organic materials are interesting and useful in optoelectronic devices. However, many known fluorescent organic molecules having π conjugate system with planar structure exhibit weak or no emission in the solid state, because the strong intermolecular interaction causes an aggregation-caused emission quenching (ACEQ) [1]. Quenching in the solid state is due to a non-radiative deactivation process, such as excimer formation, excitonic coupling, and excitation energy migration [2-3]. For example, the π–π stacking interaction between the perylene molecules prompts the formation of excimers, resulting in ACEQ effect. To overcome this problem, the prevention of the π–π stacking interaction between the planar molecules is an alternative approach.

Siloles or Silacyclopentadienes, a group of silicon containing five-membered cyclic dienes, are organic semiconducting molecules and has the lowest LUMO energy level due to the σ*-π* conjugation arising from the interaction between the σ* orbital of two exocyclic bonds on the silicon atom and the π* orbital of the butadiene moiety compared with other common five-membered heterocyclic compounds [4-10]. Due to the lowest LUMO energy level, siloles exhibit high

electron acceptability and fast electron mobility. This unique optical and electrical property are useful in various applications, such as electron transporting materials [11], light-emitting diodes (LEDs) [12-14], chemical sensors [15-16], and flexible memory storage [17]. Siloles, which is first molecules exhibited aggregation-caused emission enhancement (AIEE), are π-electron systems containing four phenyl groups in a cyclic 5-membered ring and aggregation of silole molecules restrict the intramolecular motions of the phenyl luminophores, which block the non-radiative decay channels and enhance their PL efficiencies [18]. On the other hand, nanoaggregate of silole has a surprising increase in PL efficiency when it nanoaggregates in water [19-21].

We previously reported that the polysilole could be shown to have potential as chemo-sensors for detecting explosives [15-16]. Because explosives such as 1,3,5-trinitrotoluene (TNT) are electron deficient compounds due to nitro moiety in a molecule, photoluminescence (PL) of silole decreases via electron transfer quenching. Herein, we report AIEE property of the silole nanoaggregates and their use for the detection of TNT.

1.2. Experiments

Fluorescence emission spectrum were recorded with the use of a Perkin-Elmer luminescence spectrometer LS 50B. The solvents were determined to be free of emitting impurities prior to use. To avoid changing the concentrations of the emitting compound, the experiments were carried out with solution by preparing the quencher in the same solution of the emitting compound. Dynamic light scattering (DLS) measurement was conducted by employing a DLS-8000HL (Otsuka Electronics, Japan) with 10 mW He-Ne Laser (Max 30m W), photomultiplier tube detector, and silicon photodiode monitor detector. Absolute PL quantum yield (QY) was obtained by using a Quantaurus-QY Absolute PL quantum yield spectrometer C11347-11 (Hamamatsu, Japan) with of 150 W xenon monochromatic light source, multichannel Czerny-Turner type spectroscope, and 3.3 inch spectral on integrating sphere.

1.3. Results and Discussion

The preparation method of dimethylsilole was previously reported [10]. dimethylsilole weakly emit PL at 464 nm in THF solution with excitation at 360 nm. Previously reported relative quantum yield of dimethylsilole in THF was 0.1% [22]. However absolute quantum yield (QY) of dimethysilole is 0.4% in THF. To prepare dimethylsilole nanoaggregates, the mother solution was prepared by dissolving 10 mg of dimethylsilole in 100 mL THF. The dimethylsilole nanoaggregates were prepared by rapid injection of 1 mL dimethylsilole solution into a different proportions ratios of THF and distilled water such as THF:H_2O = 0:9, 1:8, 2:7, and so forth. Figure 1.1 exhibits chemical structure of dimethylsilole (a) and illustration for excitation and emission of silole molecule (b) and nanoaggregate (c).

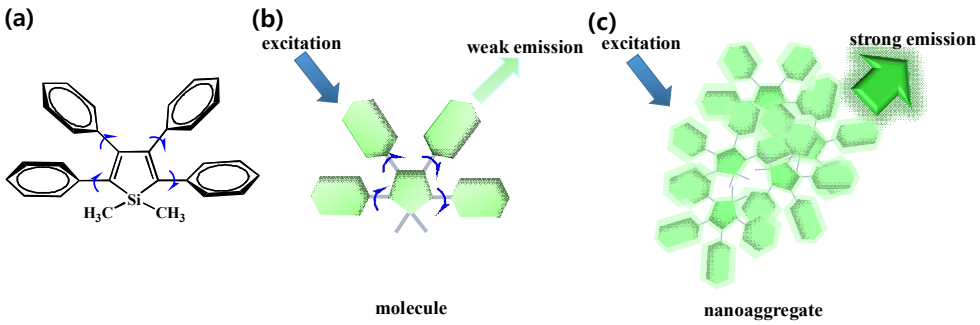

Figure 1.1 Chemical structure and illustration for excitation and emission of silole molecule and silole nanoaggregate.

PL spectra of dimethylsilole molecule and nanoaggregate are shown in Figure 1.2(a). Absolute QY of dimethylsilole molecule without aggregation and its nanoaggregate in 90% water volume fraction are 0.4% and 27.1%, respectively.

QY of dimethylsilole nanoaggregate increases more than 68 times, which is greater than that of bis(methyltetraphenyl)silole nanoaggregate [23]. Critical water concentration for onset of aggregation is measured. PL spectra of dimethylsilole nanoaggregate vs % water by volume in water-THF mixtures are shown in Figure 1.2(b). PL intensity of dimethylsilole molecule without aggregation is very weak near 464 nm. In solutions between 0% and 70% water by volume, the PL intensity of dimethylsilole does not increased. However, the PL intensity increases over 70% water by volume, which indicates the onset of aggregation. As the water fraction is increased over 80% water by volume, the PL intensity increases dramatically with no shift in the emission wavelength. Critical water concentration for the formation of nanoaggregate is a minimum volume-fraction of 70% water. Figure 1.2(c) shows the plot for the relative PL intensity of dimethylsilole nanoaggregates vs % water by volume. A photograph of dimethylsilole nanoaggregate vs % water by volume in water-THF mixtures are shown in Figure 1.2(d).

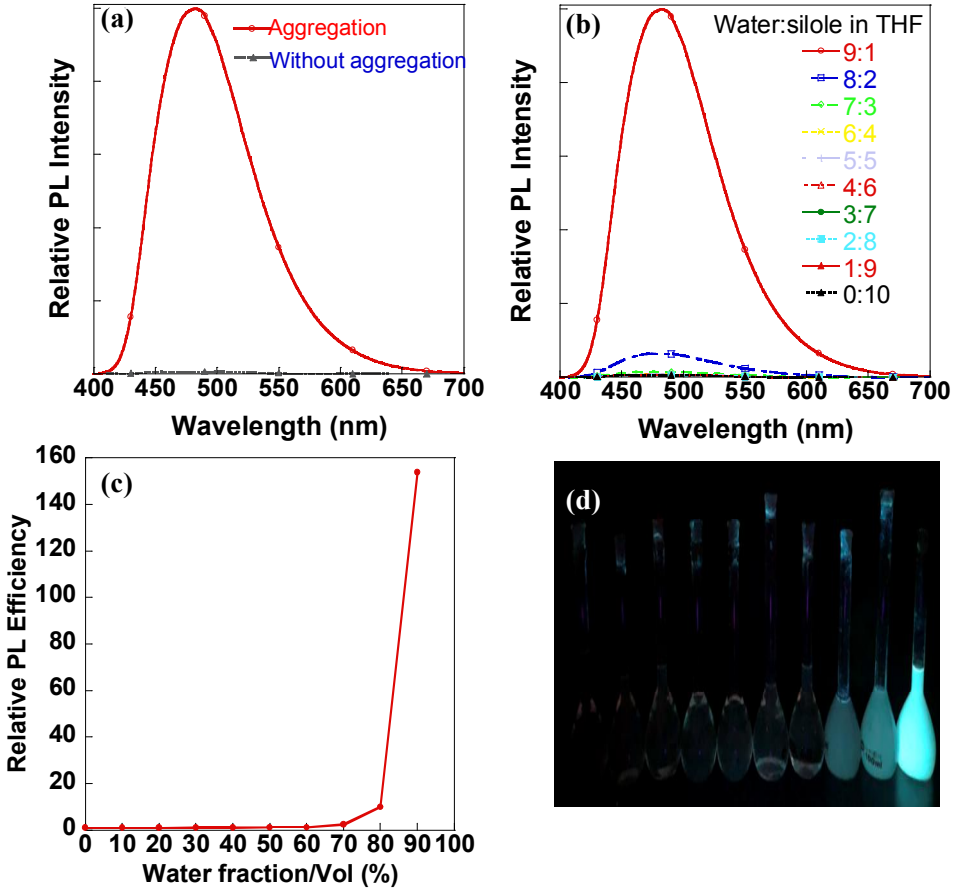

Figure 1.2 PL spectra of dimethylgermole molecule without aggregation and its nanoaggregate (a). PL spectra of dimethyleilole nanoaggregate in water-THF mixtures (% water from top; 90%, 80%, 70%, 60%, 50%, 40%, 30%, 20%, 10%, 0%) (b). Plot of the relative intensity of dimethylsilole nanoaggregate vs % water by volume and their photograph (c and d).

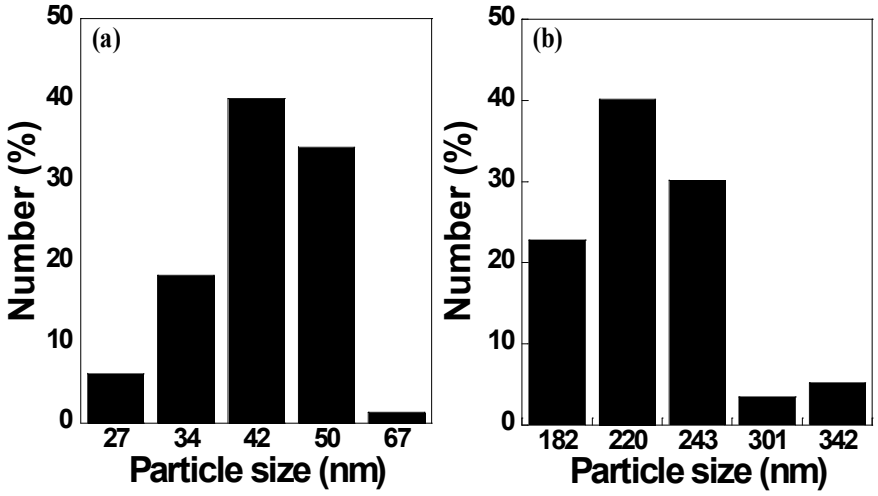

Figure 1.3 DLS data showing an increase in size when the water fraction ratio decreases to 90% (a) and 80% (b).

Figure 1.3, obtained by dynamic light scattering (DLS) measurements shows the size of nanoaggregate and size distribution in different water fractions. Particle diameter decreases as water fraction increases. Average particle diameters of dimethylsilole nanoaggregate are 35 and 257 nm as the water volume fraction decreases 90 to 80%, respectively. Average particle size of dimethylsilole nanoaggregate decreases dramatically and shows a minimum in size at 90% water. Decrease of particle size at higher water concentrations is due to the hydrophobicity of organic molecules.

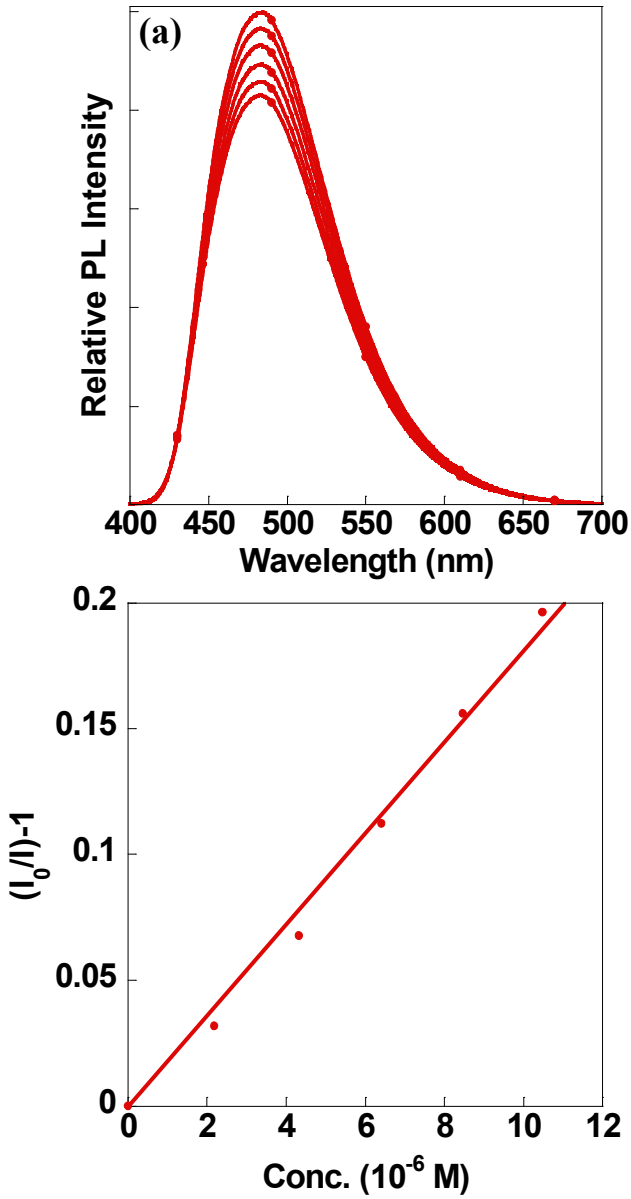

Figure 1.4 Quenching PL spectra of increasing fraction by 500 part per billion (ppb) of each TNT concentration in dimethylsilole nanoaggregates solution (a) and Stern-Volmer plot showing sensing efficiency for dimethylsilole nanoaggregate (b).

Dimethylsilole nanoaggregate with a volume-fraction of 90% water is utilized to detect trinitrotoluene (TNT). PL quenching is measured by adding successive aliquots of an identical volume-fraction of 90% water stock solution of TNT to the nanoaggregate. The decrease in PL intensity is measured as a function of added TNT. Quenching PL spectra by adding 500 part per billion (ppb) of each TNT concentration in dimethylsilole nanoaggregates solution are shown in Figure 4(a). The response of quenching PL intensity of dimethylsilole nanoaggregate to TNT is analyzed using the Stern-Volmer equation [24]: $I_0/I = K_{SV}[Q] + 1$. In this equation, I is the PL intensity at quencher concentration, [Q], I0 is the PL intensity at [Q] = 0, and K_{SV} is the Stern-Volmer constant. Linear Stern-Volmer relationship is observed for the dimethylsilole nanoaggregatele for the detection of TNT in the ppb range as shown in Figure 4(b).

Stern-Volmer constant (K_{SV}) of dimethylsilole nanoaggregate for TNT indicating detection efficiency was 18,000 M^{-1}. Previously we reported that the Stern-Volmer constant of non-aggregate silole polymer, poly(tetraphenyl)siloles [16], and bis(methyltetraphenyl)silole nanoaggregate [23] for TNT detection were 4,350 and 26,000 M^{-1}, respectively [16]. Trogler et al. reported that the Stern-Volmer constant of oligo(tetraphenyl)silole nanoaggregate with a volume-fraction of 90% water was 4,100 M^{-1} [25]. Detection efficiency of dimethylsilole nanoaggregate to TNT is greater than that of non-aggregated polysilole in THF solution but less than that of bis(methyltetraphenyl)silole nanoaggregate. The better detection efficiency and higher absolute QY of bis(methyltetraphenyl)silole might be due to the conjugation extension through the Si-Si bond in bis(methyltetraphenyl)silole.

1.4. Conclusions

Aggregation-induced emission property of dimethylsilole nanoaggregates and its successful sensing of explosive were reported. Absolute QY of dimethylsilole molecule without aggregation and its nanoaggregate in 90% water volume fraction are 0.4% and 27.1%, respectively. QY of dimethylsilole nanoaggregate increases more than 68 times. Critical water concentration for the formation of nanoaggregate is a minimum volume-fraction of 70% water. Average particle diameters of dimethylsilole nanoaggregate are 35 nm at 90% water. The dimethylsilole nanoaggregates used for the detection of TNT and showed greater sensitivity. Stern-Volmer constant (K_{SV}) of dimethylsilole nanoaggregate for TNT was 18,000 M^{-1}. Detection efficiency of dimethylsilole nanoaggregate to TNT is greater than that of non-aggregated silole.

1.5. References

[1] G. M. Fischer, E. Daltrozzo and A. Zumbusch, *Angew. Chem., Int. Ed.* 50, 1406 **(2011)**.

[2] S. A. Jenekhe and J. A. *Osaheni, Science* 265, 765 **(1994)**.

[3] Z. R. Grabowski and K. Rotkiewicz, *Chem. Rev.* 103, 3899 **(2003)**.

[4] A.P. Sadimenko, *Adv. Heterocycl. Chem.* 79, 115 **(2001)**.

[5] V.Y. Lee, A. Sekiguchi, M. Ichinohe, N. Fukaya, *J. Organomet. Chem.* 611, 228 **(2000)**.

[6] K. Tamao, M. Uchida, T. Izumizawa, K. Furukawa, S. Yamaguchi, *J. Am. Chem. Soc.* 118, 11974 **(1996)**.

[7] S. Yamaguchi, K. Tamao, *J. Chem. Soc., Dalton Trans.* 3693 **(1998)**.

[8] B. Wrackmeyer, Coord. *Chem. Rev.* 145, 125 **(1995)**.

[9] C. Chuit, R.J.P. Corriu, C. Reye, J.C. Young, *Chem. Rev.* 93, 1371 **(1993)**.

[10] R. West, H. Sohn, U. Bankwitz, J. Calabrese, Y. Apeloig and T. Mueller, *J. Am. Chem. Soc.* 117, 11608 **(1995)**.

[11] K. Tamao, M. Uchida, T. Izumizawa, K. Furukawa and S. Yamaguchi, *J. Am. Chem. Soc.* 118, 11974 **(1996)**.

[12] H. Sohn, R. R. Huddleston, D. R. Powell and R. West, *J. Am. Chem. Soc.* 121, 2935 **(1999)**.

[13] Y. Xu, T. Fujino, H. Naito, T. Dohmaru, K. Oka, H. Sohn and R. West, *Jpn. J. Appl. Phys.* 38, 6915 **(1999)**.

[14] Y. H. Park, Y. Kim and H. Sohn, *J. Korean Phys. Soc.* 59, 2318 **(2011)**.

[15] H. Sohn, R. M. Calhoun, M. J. Sailor and W. C. Trogler, *Angew. Chem. Int. Ed.* 40, 2104 **(2001)**.

[16] H. Sohn, M. J. Sailor, D. Magde and W. C. Trogler, *J. Am. Chem. Soc.* 125, 3821 **(2003)**.

[17] J.-K. Choi, S. Jang, K.-J. Kim, H. Sohn and H.-D. Jeong, *J. Am Chem. Soc.* 133, 7764 **(2011)**.

[18] J. Luo, Z. Xie, J. W. Y. Lam, L. Cheng, H. Chen, C. Qiu, H. S. Kwok, X. Zhan, Y. Liu, D. Zhu and B. Z. Tang, *Chem. Commun*.1740 **(2001)**.

[19] S. Jang, S. G. Kim, D. Jung, H. Kwon, J. Song, S. Cho, Y. C. Ko and H. Sohn, *B. Kor. Chem. Soc.* 27, 1965 **(2006)**.

[20] L. C. Palilis, A. J. Maekinen, M. Uchida and Z. H. Kafafi, *Appl. Phys. Lett.* 14, 2209 **(2003)**.

[21] B.-K. An, S.-K. Kwon, S.-D. Jung, and S. Y. Park, *J. Am. Chem. Soc*. 124, 14410 **(2002)**.

[22] H. J. Tracy,. J. L. Mullin, W. T. Klooster, J. A. Martin, J. Haug, S. Wallace, I. Rudloe and K. Watts, *Inorg. Chem*. 44, 2003 **(2005)**.

[23] B. Shin and H. Sohn, *J. Korean Phys. Soc*. 72, 234 **(2018)**.

[24] N. J. Turro, Modern Molecular Photochemistry, U*niversity Science Books, Sausalito, California,* **(1991)**.

[25] S. J. Toal, D. Magde and W. C. Trogler, *Chem. Commun*. 5465 **(2005)**.

PART 2

Heavy Atom Effect on Metallole Nanoaggregates and Their Explosive Sensing Applications

2.1. Introduction

Molecules having high emission properties in the solid state have recently attraction due to their unique optical properties, which could be achieved from the reduction of a non-radiative process and excimer formation. Since the most of the high fluorescent organic molecules are flat-conjugated molecules, they prefer to be a fluorescence quenching due to the strong intermolecular stacking interaction in the solid state. To overcome this problem, the structure of the fluorescence molecules should provide a prevention of stacking interaction by the restricted rotation of the aromatic rings in the solid state, which is an aggregation-induced emission enhancement (AIEE) [1,2].

Siloles are first example which proves AIEE properties [3]. Siloles have an unique electronic properties [4,5,6], which could be applied in various fields, such as electron transporting materials [7], light-emitting diodes (LEDs) [8,9,10], chemical sensors [10,11], and flexible flexible memory storage [12]. Metalloles have a structure with π-electron systems containing M (M = Si, Ge, and Sn) as a part of cyclic 5-membered ring. Metallole has a quite low-lying LUMO level, which is ascribed to the σ*-π* conjugation in the ring, that is, the orbital

interaction between the σ* orbital of the two exocyclic bonds on the metal with the π* orbital of the butadiene moiety [13]. Germoles and stannoles, however, have received much less attention as AIEE units. Herein, we are interested in the AIEE properties of the π-conjugated systems containing the heavier group 14 metalloles, i.e., germole and stannole, and particularly in the AIEE effects of the central group 14 elements on their electronic structures. We report synthesis and optical characterization of germole and stannole nanoaggregates. Those nanoaggregates showing high PL efficiency through AIEE exhibited the high efficiency in sensing explosives. An AIEE of germole and stannole nanoaggregates and their Stern-Volmer analyses for the comparison of the detection efficiencies of explosives are reported.

2.2. Experimental Details

2.2.1. General

All synthetic manipulations were carried out under an atmosphere of dry argon gas using standard vacuum-line Schlenk technique. All solvents were purified and degassed before use according to standard literature methods: diethylether, tetrahydrofuran (THF), n-hexane, and ethanol were purchased from Aldrich Chemical Co. Inc. and distilled from sodium/benzophenone ketyl. All other reagents (Aldrich) such as diphenylacetylene, lithium wire, and dimethyldichlorotin were purchased and used without any purification. Spectroscopic grade THF from Fisher Scientific was used for the fluorescence measurements. The concentration of metallole nanoaggregates for the fluorescence measurement was 10 mg/100 mL. 1,3,5-trinitrotoluene (TNT) was prepared from 2,4-dinitrotoluene (DNT) and recrystallized twice from methanol.

2.2.2. Synthesis of Dimethyltetraphenylgermole(Germole) and Dimethyltetraphenylstannole(Stannole)

Diphenylacetylene (26.7 g, 150 mmol) and lithium (1.38 g, 200 mmol) were stirred in diethyl ether (150 mL) at room temperature for 3.5 h. The reaction gave a brown solution and a yellow precipitate. The solution was frozen with a bath of liquid nitrogen, after removal of lithium metal. Me_2GeCl_2 (52.2 g, 300 mmol) was added by a syringe in one portion. The mixture kept at -196°C of 5 min before the cooling bath was removed, and the solution was allowed to warm up slowly to room temperature, and stirred for 4 h to give a yellow solution. The solution was cannulated, concentrated, and crystalized at -20°C to give

product as yellow crystals ($Ph_4C_4GeMe_2$, isolated yield: 27.55 g, 80%) at -10°C. Selected data for $Ph_4C_4GeMe_2$: 1H NMR (300 MHz, $CDCl_3$ (δ= 7.24)): δ=6.79-7.12 (br. m, 20H, Ph), 0.66 (s, 6H, CH3).

The procedure for synthesizing Me_2SnCl_2 was similar to that for. For $Ph_4C_4SnMe_2$, Me_2SnCl_2 (65.9 g, 300 mmol) was added by a syringe in one portion. ($Ph_4C_4SnMe_2$, isolated yield: 30.3 g, 80%). Selected data for $Ph_4C_4SnMe_2$: ^{1}H NMR (300 MHz, CDCl3 (δ= 7.24)): δ=6.7-7.2 (br. m, 20H, Ph), 0.6 (s, 6H, CH_3)

2.2.3. Instrumentation and Data Acquisition

Fluorescence emission spectrum were recorded with the use of a Perkin-Elmer luminescence spectrometer LS 50B. The solvents were determined to be free of emitting impurities prior to use. A composition of analyte solution was identical with a composition of nanoaggregate solution. Absolute PL quantum yield (QY) was obtained by using a Quantaurus-QY Absolute PL quantum yield spectrometer C11347-11 (Hamamatsu, Japan) with of 150 W xenon monochromatic light source, multichannel Czerny-Turner type spectroscope, and 3.3 inch spectral on integrating sphere. Sizes of stannole nanoaggregates were obtained by Dynamic light scattering (DLS) measurement was conducted by employing a DLS-8000HL (Otsuka Electronics, Japan) with 10 mW He-Ne Laser (Max 30 mW). The UV-vis spectra were obtained with the use of a Shimadzu, UV-1650PC (Shimadzu, Tokyo, Japan) spectrometer.

2.3. Results and Discussion

2.3.1. Photophysical Propertis of Metalloles

The UV-vis absorption and fluorescence spectral data for the germole and stannole are shown in Figure 2.1. The metalloles exhibit an absorption band, which is ascribed to the π-(σ*-π*) transitions in the metallole ring. Absorptions at a wavelength of 356 nm for the germole and 354 nm for the stannole are assigned to the metallole π-(σ*-π*), which are about 14 to 16 nm blue-shifted, relative to that of poly(tetraphenyl)silole.[12] These blue shifts are attributed to partial conjugation of the phenyl groups to the metallole ring without the σ-σ* conjugation of polymer main chain.

The fluorescence measurement of the germole and stannole exhibit one emission band at 457 and 478 nm with an excitation at 350 nm, respectively. Emission peak for the stannole is red-shifted by 21 nm, compared to that of the germole. This result indicates that the longer distance between carbon and tin causes the less efficient interaction between the π* orbital of carbon with the σ* orbital of tin in the stannole ring. Absolute quantum yield (QY) of the germole and stannole are measured in THF and exhibit 0.3% and 0.1%, respectively. The quantum yield of the germole is three times higher than that of the stannole, which is due to the heavy element effect of tin.

2.3.2. Amplified Phtoluminescence of Metallole Nanoaggregates

Although many types of silole nanoaggregates are studied, there is no investigation on heavy atom effect [16]. Previously we reported the behaviors of silole nanoaggregates [17,18]. It might be interesting to investigate the behaviors of metallole nanoaggregates as a central atom becomes heavier in the metallole

ring. To prepare the nanoaggregates, the mother solution was prepared by dissolving 10 mg of metallole in 100 mL THF. The metallole nanoaggregates were prepared by rapid injection of 1 mL metallole solution into different proportion ratios of THF and distilled water mixture solution (1 mL), such as THF:H2O=0:9, 1:8, 2:7, and so forth. Figure 2.2.A shows the relative PL spectra of germole nanoaggregate in water-THF mixtures (water % from top; 90%, 80%, 70%, 60%, 50%, 40%, 30%, 20%, 10%, 0%). Figure 2.2.B shows the relative PL spectra of stannole nanoaggregate in water-THF mixtures.

Figure 2.2.C shows the PL efficiency of germole and stannole nanoaggregate vs % water by volume. The germole and stannole nanoaggregates in 90% water fraction exhibit one emission band at 467 and 490 nm with an excitation at 350 nm, respectively. The emission bands of germole and stannole nanoaggregates red-shifts slightly by 10 and 12 nm relative to molecule in THF solution, respectively. This suggests that the metallole nanoaggregates exhibit neither -stacking of phenyl group nor excimer formation in colloid solution. The PL efficiency of germole and stannole nanoaggregates does not increased until 70% water by volume. However, the PL efficiency increases dramatically over 70% water by volume, which indicates the onset of aggregation. This is due to result from the steric effect and the restriction of intramolecular rotations in the aggregates. The relative intensity of the PL for the germole and stannole nanoaggregates increases by about 28 and 18 times, respectively, when the solution is 90% water by volume.

Interestingly, the PL intensity of metallole nanoaggregates in 99% water by volume decreases, which is probably due to the precipitation of metallole in high water content. Absolute quantum yield of germole and stannole nanoaggregates in 90% water were 5.9% and 1.4%, respectively. Increase of absolute quantum yield in nanoaggregate is similar to the result obtained from the relative PL intensity.

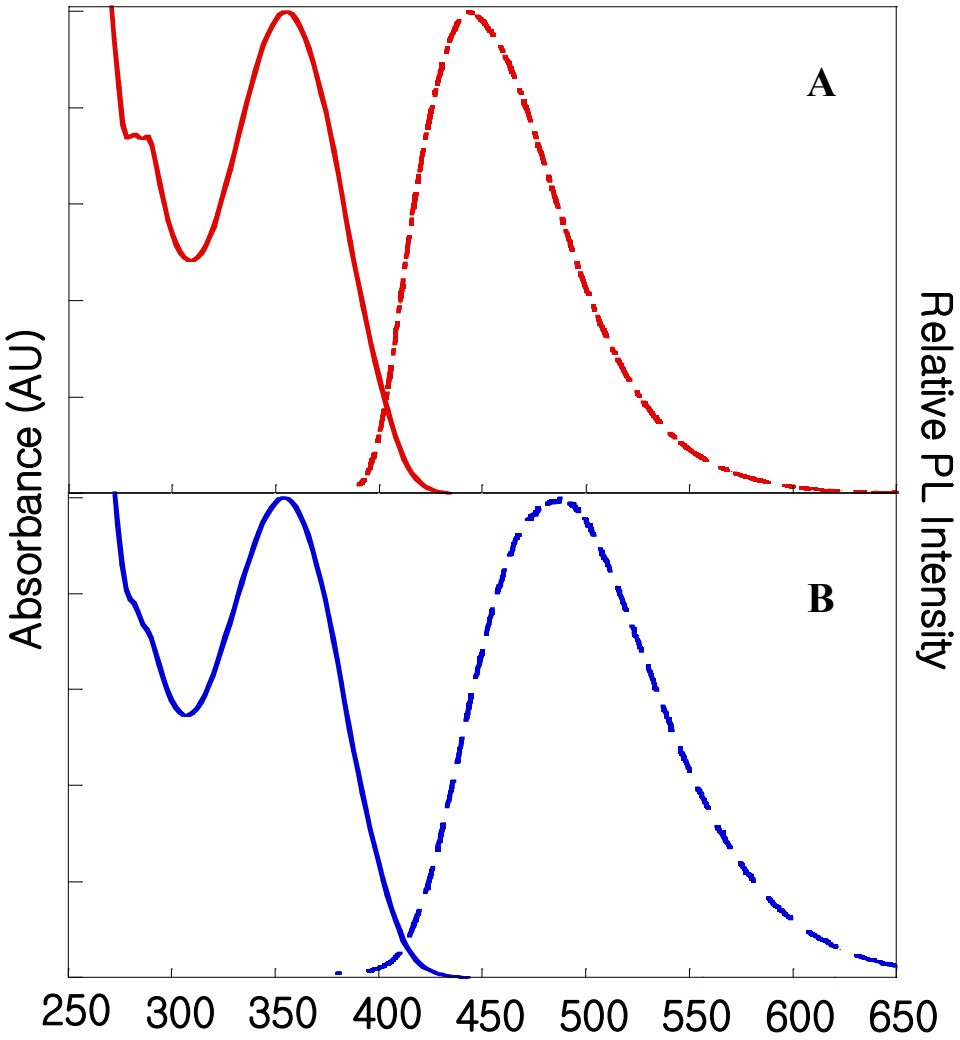

Figure 2.1 UV-vis absorption spectra (solid line) and fluorescence spectra in THF in (dotted line) for (A) dimethyltetrapnenylgermole and (B) dimethyltetraphenylstannole.

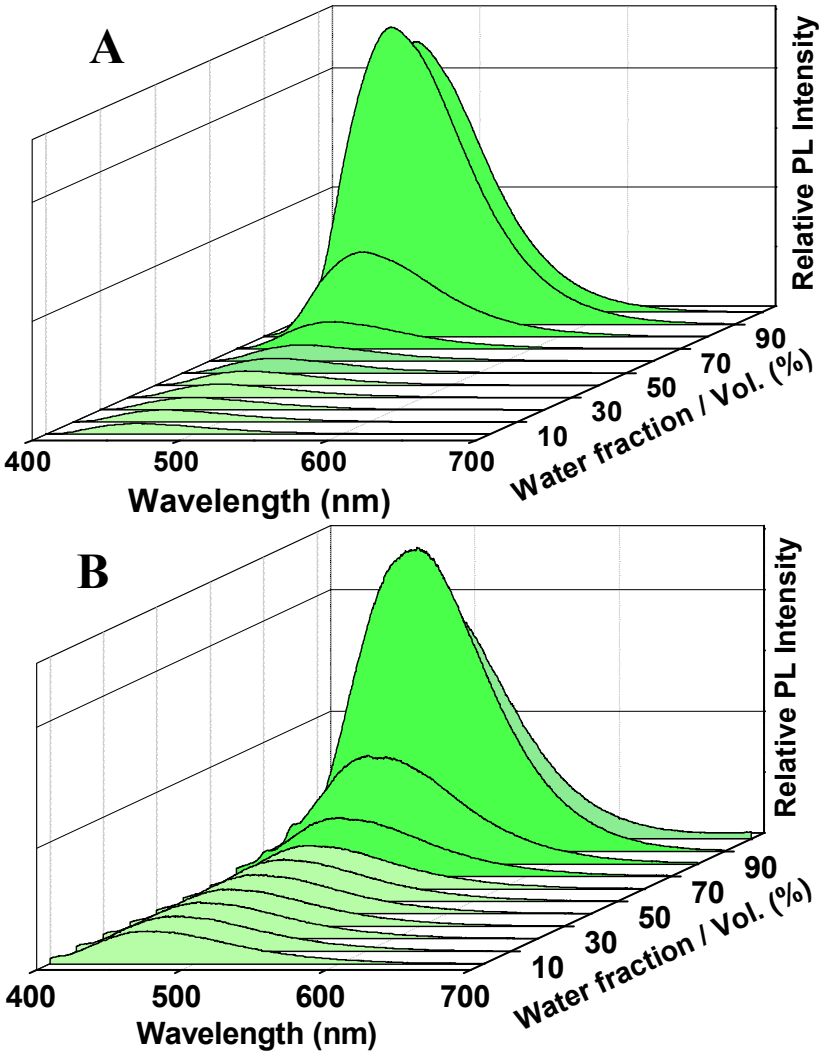

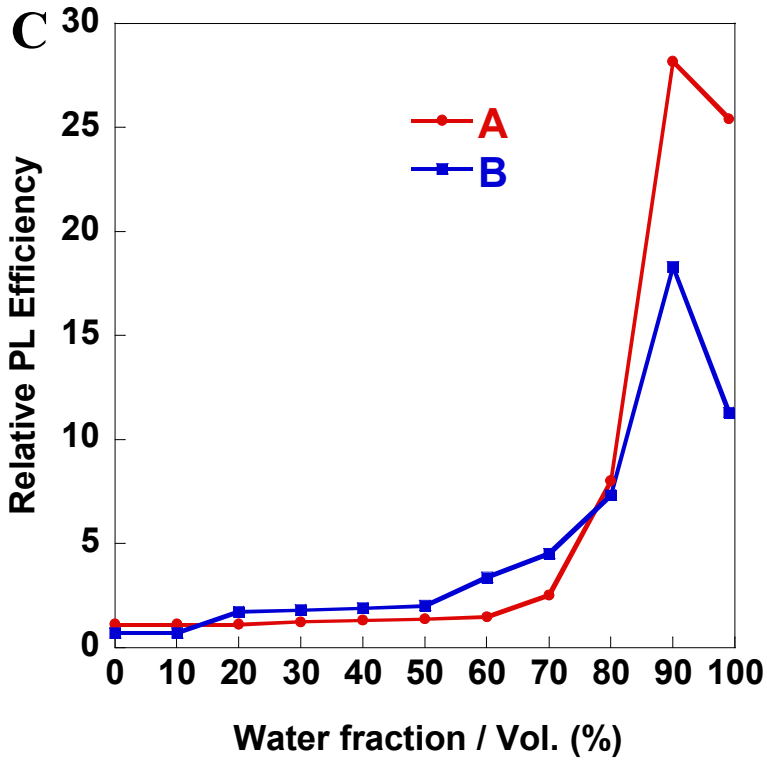

Figure 2.2 PL spectra of germole (A) and stannole (B) nanoaggregates in water-THF mixtures (99%, 90%, 80%, 70%, 60%, 50%, 40%, 30%, 20%, 10%, 0%). Plot of the relative intensity of germole nanoaggregate (red) and stannole nanoaggregate (blue) versus % water by volume (C).

Figure 2.3, obtained by dynamic light scattering measurements shows the size of nanoaggregate in different water fractions. Particle diameter and dispersity of diameter decrease as water fraction increases. Both nanoaggregates exhibit a minimum in size at 90% water. Average particle diameters for germole and stannole nanoaggregates at 90% water are 46 and 42 nm, respectively. This result is very similar to previously reported data [15]. However average particle diameters for germole and stannole nanoaggregates at 99% water increase slightly and are 56 and 60 nm, respectively. This result correlates very well with the relative PL efficiency in metallole nanoaggregates.

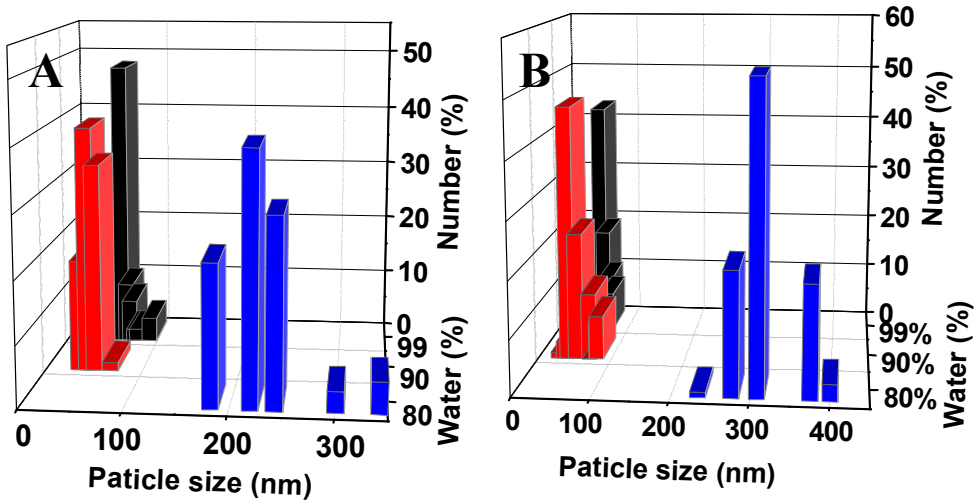

Figure 2.3. DLS data showing an average particle diameter at the water fraction ratio of 99%, 90%, and 80% for germole nanoaggregates (A) and stannole nanoaggregates (B).

2.3.3. Photoluminescence Quenching Studies with TNT

The sensing studies of the germole and stannole nanoaggregates at 90% water volume-fraction for TNT were investigated. The PL quenching by adding successive aliquots of an identical volume-fraction of 90% water of TNT stock solution to the nanoaggregate was achieved. Figure 2.4A and 2.4B show the quenching PL spectra upon addition of 500 part per billion (ppb) of each TNT. The PL quenching efficiencies of the germole nanoaggregates is greater than that of stannole nanoaggregates. The responses to quenching between both nanoaggregates were analyzed using the Stern-Volmer equation: $I_0/I = K_{SV}[Q] + 1$. In this equation, I is the fluorescence intensity at quencher concentration, [Q], I_0 is the intensity at [Q] = 0, and K_{SV} is the Stern-Volmer constant. Linear Stern-Volmer relationships are observed for both nanoaggregates. Stern-Volmer constant of germole and stannole nanoaggregates for TNT were 8,200 and 1,600

M^{-1}, respectively. Previously we reported that the Stern-Volmer constant for poly(tetraphenyl)siloles was about 4,350 M^{-1} [11]. This result indicates that metallole nanoaggregates could be useful to detect nitroaromatic compounds.

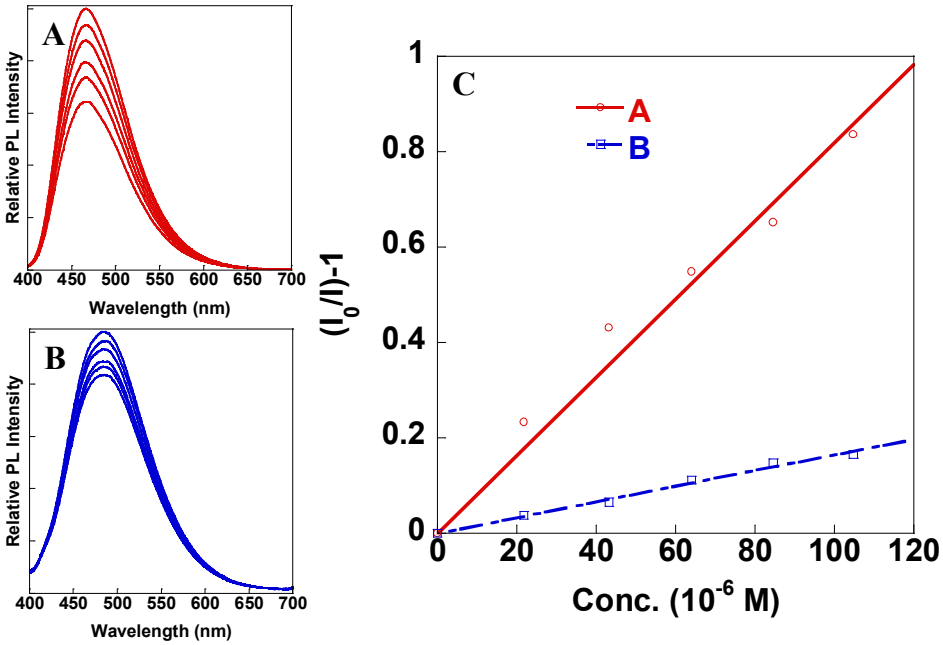

Figure 2.4 Quenching PL spectra upon addition of 500 part per billion (ppb) of each TNT for germole nanoaggregates (A) and stannole nanoaggregates (B). Stern−Volmer plot showing sensing efficiency for both nanoaggregates (C).

2.4. Conclusions

The AIEE properties of the heavier group 14 metalloles such as germole and stannole nanoaggregate are reported. The fluorescence measurement indicated that the emission peak for the germole is blue-shifted and the absolute QY of the germole is higher than that of the stannole, which is due to the heavy element effect of tin. Thus the AIEE property decreases as the central atom becomes heavier in the metallole ring. The germole and stannole nanoaggregates in 90% water fraction exhibit maximum PL efficiency with minimum particle size. The sensing studies of the germole and stannole nanoaggregates at 90% water volume-fraction for TNT indicate that the germole nanoaggregates exhibits better detection efficiency.

2.5. References

[1] J. Mei, N. L. C. Leung, R. T. K. Kwok, J. W. Y. Lam, and B. Z. Tang, *Chem. Rev*. 115, 11718 **(2015)**.

[2]. J. Mei, Y. Hong, J. W. Y. Lam, A. Qin, Y. Tang, and B. Z. Tang, *Adv. Mat*. 26, 5429 **(2017)**.

[3]. J. Luo, Z. Xie, J. W. Y. Lam, L. Cheng, H. Chen, C. Qiu, H. S. Kwok, X. Zhan, Y. Liu, D. Zhu, and B. Z. Tang, *Chem. Commun*.1740 **(2001)**.

[4]. R. West, H. Sohn, U. Bankwitz, J. Calabrese, Y. Apeloig, and T. Mueller, *J. Am. Chem. Soc*. 117, 11608 **(1995)**.

[5]. H. Sohn, D. R. Powell, R. West, J.-H. Hong, and W.-C. Joo, *Organometallics* 16, 2770 **(1997)**.

[6]. S. Yamaguchi and K. Tamao, *J. Chem. Soc., Dalton Trans.* 3693**(1998)**.

[7]. K. Tamao, M. Uchida, T. Izumizawa, K. Furukawa, and S. Yamaguchi, *J. Am. Chem. Soc*. 118, 11974 **(1996)**.

[8]. H. Sohn, R. R. Huddleston, D. R. Powell, and R. West, *J. Am. Chem. Soc*. 121, 2935 **(1999)**.

[9]. Y. Xu, T. Fujino, H. Naito, T. Dohmaru, K. Oka, H. Sohn, and R. West, *Jpn. J. Appl. Phys*. 38, 6915 **(1999)**.

[10]. Y. H. Park, Y. Kim, and H. Sohn, *J. Korean Phys. Soc*. 59, 2318 **(2011)**.

[11]. H. Sohn, M. J. Sailor, D. Magde, and W. C. Trogler, *J. Am. Chem. Soc*. 125, 3821 **(2003)**.

[12]. J.-K. Choi, S. Jang, K.-J. Kim, H. Sohn, and H.-D. Jeong, **J. Am Chem. Soc**. 133, 7764 **(2011)**.

[13]. S. Yamaguchi, Y. Itami, and K. Tamao, Organometallics 17, 4910 **(1998)**.

[14]. J. W. H. Dennis, D. H.Rosenblatt, W. G. Blucher, C. L. Coon, *J. Chem. Eng*. Data 20, 202 **(1975)**.

[15]. S. Jang, S. G. Kim, D. Jung, H. Kwon, J. Song, S. Cho, Y. C. Ko, and H. Sohn, *B. Kor. Chem. Soc*. 27, 1965 **(2006)**.

[16]. Q. Zeng, Y. Dong, C. Di, A. Qin, Y. Hong, L. Ji, Z. Zhu, C. K. W. Jim,

G. Yu, Q. Li, Z. Li, Y. Liu, J. Qin, and B. Z. Tang, *Chem. Commun.* 70, **(2007)**.

[17]. B. Shin and H. Sohn, *J. Korean Phys. Soc*. 72, 234 **(2018)**.

[18]. B. Shin and H. Sohn, *J. Nanosci. Nanotechnol*. 19, 991 **(2019)**

PART 3

TNT Sensor Based on Silole Nanoaggregates

3.1 Introduction

Materials with high emission are very intriguing and highly demanded in optical and electronic devices. Previously developed materials with known fluorescent molecules exhibited high fluorescence in dilute solution exhibit low or no emission in the solid state, because the strong intermolecular π–π stacking interaction causes an aggregation-caused emission quenching (ACEQ) [1]. The ACEQ is generally attributed to a nonradiative deactivation process, such as excitonic coupling, excimer formation, and excitation energy migration to the impurity traps [2,3]. Since the most of the fluorescent molecules are donor-acceptor type or flat π-conjugated molecules, they are more prone to molecular aggregation and fluorescence quenching in the solid state [4,5].

Decrease of emission efficiency in the solid state has been a major problem in optical device applications. Many attempts through chemical, physical, and engineering approaches have been made to prevent the formation of less emissive species. To overcome this problem, an aggregation-induced emission enhancement (AIEE) is an alternative approach is to control the fluorescence properties in the solid state. Recently, many aromatic AIEE compounds have been reported [6].

Siloles have recently attracted much attention due to its unique electronic properties [7,8]. The unique optical and electrical phenomenon could be applied in various fields, such as electron transporting materials,9 light-emitting diodes (LEDs) [10-12], chemical sensors [13,14], and flexible memory storage[15]. Siloles is structured with π-electron systems containing Si atom as a part of cyclic 5-membered ring that shows an AIEE [16]. These non-emissive molecules

are induced to be efficiently emissive by aggregate formation. The above effect of aggregation shows opposite behavior from the one observed in common luminophore systems, where aggregate formation usually cause decrease in PL efficiency. On the other hand, nanoaggregate has a surprising increase in PL efficiency when it nanoaggregates in water[17-19]. AIEE has been attributed by the restricted rotation of the phenyl rings, which limits the nonradiative decay pathways [20].

Sensors offering new approaches to the rapid detection of ultra-trace anaytes from explosives, have attracted attention because explosives are important chemical species to detect in mine fields, forensic investigations, and homeland security applications. Silole have also been shown to have potential as chemo-sensors for detecting explosives.14 Because explosives such as 1,3,5-trinitrotoluene (TNT) are electron deficient compounds due to nitro moiety in a molecule, photoluminescence (PL) of silole decreases via electron transfer quenching.

Herein, we report synthesis and optical characterization of two different types of silole fluorophore nanoaggregates such as silole nanoaggregate and silole-siloxane nanoaggregate. Evidently, those nanoaggregates showing high PL efficiency through AIEE, would have the high efficiency in sensing explosives. An AIEE of silole and silole-siloxane nanoaggregates and their Stern-Volmer analyses for the comparison of the detection efficiencies of explosives are reported.

3.2 EXPERIMENTAL DETAILS

3.2.1. General

All synthetic manipulations were carried out under an atmosphere of dry argon gas using standard vacuum-line Schlenk technique. All solvents were purified and degassed before use according to standard literature methods: diethylether, tetrahydrofuran (THF), n-Hexane, ethanol were purchased from Aldrich Chemical Co. Inc. and distilled from sodium/benzophenone ketyl. All other reagents (Aldrich) such as diphenylacetylene, lithium wire, and methyltrichlorosilane were purchased and used without any purification. Spectroscopic grade THF from Fisher Scientific was used for the fluorescence measurements. The concentration of silole nanoaggregates for the fluorescence measurement was 10 mg/100 mL.

3.2.2. Preparation of bis(methyltetraphenyl)silole

The preparation method of bis(methyltetraphenyl)silole was previously reported [21].

3.2.3. Preparation of bis(methyltetraphenyl)silole siloxane

To a solution of 1-chloro-1-methyl-2,3,4,5-tetraphenyl-1-silacyclopentadiene (4.58 g, 10 mmol) in THF (200 mL) was added H_2O (0.18 g, 10 mmol) and triethlyamime(1.01 g, 10 mmol) After stirred at room temperature for 24 hrs. After evaporating THF from the mixture, the remaining solid was treated with water and diethylether. The organic layer was separated and dried ($MgSO_4$). The solvent was removed in vacuo, and the solid was washed with ethanol for purification [24].

Mp ≥ 250°C. ^{1}H NMR (300 MHz, $CDCl_3$ (δ 7.26)): δ 6.7-6.8 and 6.9-7.2 (m, 40H, Ph), 0.38 (s, 6H). 13C NMR (100 MHz, CD_2Cl_3 (δ 77.00)): δ 154.6, 139.07, 138.81, 137.34, 130.16, 129.53, 128.54, 128.08, 126.99, 126.46, -2.7.

3.2.4. Instruments and Data Acquisitions

Fluorescence emission spectrum were recorded with the use of a Perkin-Elmer

luminescence spectrometer LS 50B. The solvents were determined to be free of emitting impurities prior to use. To avoid changing the concentrations of the emitting compound, the experiments were carried out with solution by preparing the quencher in the same solution of the emitting compound. Absolute PL quantum yield (QY) was obtained by using a Quantaurus-QY Absolute PL quantum yield spectrometer C11347-11 (Hamamatsu, Japan) with of 150 W xenon monochromatic light source, multichannel Czerny-Turner type spectroscope, and 3.3 inch spectral on integrating sphere. Dynamic light scattering (DLS) measurement was conducted by employing a DLS-8000HL (Otsuka Electronics, Japan) with 10 mW He-Ne Laser (Max 30m W), photomultiplier tube detector, and silicon photodiode monitor detector.

3.3. RESULTS AND DISCUSSION

Siloles have attracted attention because of their unusual electronic and optical properties caused from extensively delocalization through silicon atom of five membered ring at LUMO level. Silole have also been shown to have potential as chemo-sensors for detecting explosives [14]. One of the characteristic optical property of silole is AIEE. AIEE is result from the steric effect of the peripheral phenyl rings caused nonplanar conformations, which prevents them from packing via π-π stacking interactions and quenching by excimers. The restriction of intramolecular rotations in the aggregates blocks the nonradiative decay, hence changing the weak emitters to strong emitters.

Two different types of nanoaggregates containing silole molecules, silole nanoaggregate and silole-siloxane nanoaggregate were provided and examined for their optical properties in nanoaggregates. Figure 3.1 shows the molecular structures and intermolecular rotations. In case of bis(methyltetraphenyl)silole, two silole units are directly connected through Si-Si bond which could cause more strict intramolecular rotation and conjugation of silicon σ bond. However, two silole units in bis(methyltetraphenyl)silole siloxane are connected by oxygen atom, which allows more flexible intramolecular rotation.

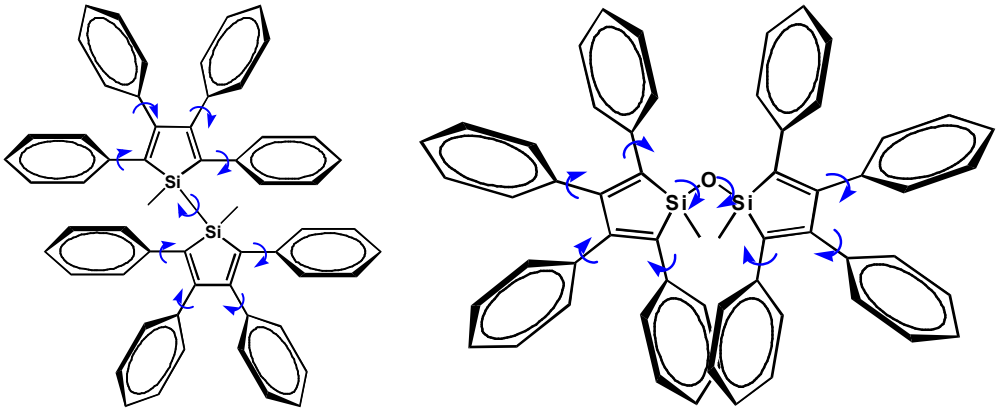

Figure 3.1 Chemical structure of bis(methyltetraphenyl)silole (left) and bis(methyltetraphenyl)silole siloxane (right).

Bis(methyltetraphenyl)silole and bis(methyltetraphenyl)silole siloxane show emission near 490 and 480 nm, when excited at 360 nm, respectively. Absolute quantum yield (QY) of bis(methyltetraphenyl)silole and bis(methyltetraphenyl)silole siloxane are measured in THF solution and exhibits 0.8% and 0.4%, respectively. This result might be due to the short conjugation of silole unit through Si-Si bond. To prepare the nanoaggregates, the mother solution was prepared by dissolving 10 mg of silole in 100 mL THF. The silole nanoaggregates were prepared by rapid injection of 1 mL silole solution into a different proportions ratios of THF and distilled water such as THF:H2O = 0:9, 1:8, 2:7, and so forth. Schematic diagram for the preparation of silole nanoaggregates is shown in Figure 3.2.

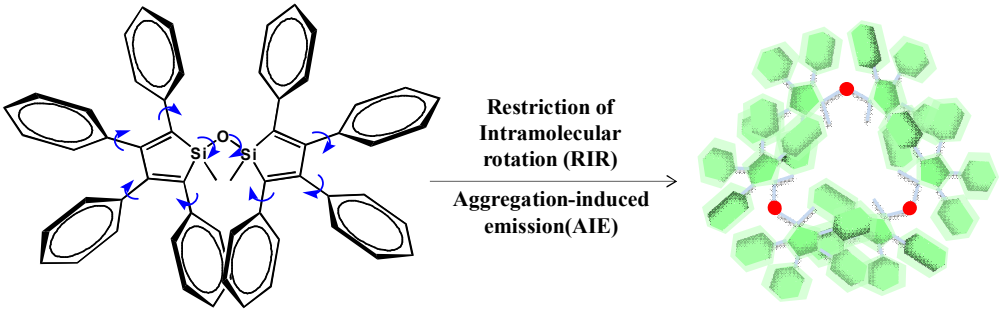

Figure 3.2 Chemical structure of bis(methyltetraphenyl)silole (left) and bis(methyltetraphenyl)silole siloxane (right).

Figure 3.3A shows the relative PL spectra of bis(methyltetraphenyl)silole nanoaggregate in water-THF mixtures (% water from top; 90%, 80%, 70%, 60%, 50%, 40%, 30%, 20%, 10%, 0%). Figure 3.3B shows the relative PL spectra of bis(methyltetraphenyl)silole siloxane nanoaggregate in water-THF mixtures. Figure 3.3C shows the PL efficiency of bis(methyltetraphenyl)silole nanoaggregate vs % water by volume. Bis(methyltetraphenyl)silole naggregate exhibits a nearly identical emission band, however the emission band of bis(methyltetraphenyl)silole siloxane nanoaggregates red-shifts by 20 nm in nanoaggregates. For bis(methyltetraphenyl)silole solution in pure THF, the PL is very weak near 490 nm. In solutions between 0% and 50% water by volume, the PL efficiency of bis(methyltetraphenyl)silole nanoaggregates does not increased. However, the PL efficiency increases over 50% water by volume, which indicates the onset of aggregation. In case of bis(methyltetraphenyl)silole siloxane nanoaggregate, the PL efficiency increases over 70% water by volume. As the water fraction is increased, the PL efficiency increases dramatically. Critical water concentration for the formation of bissilole and bissilole siloxane nanoaggregate are a minimum volume-fraction of 50% and 70% water, respectively. Since AIEE is due to result from the steric effect and the restriction of intramolecular rotations in the aggregates, more strict intramolecular rotation of bissilole exhibits lower % water of the onset of aggregation. Absolute quantum yield of bissilole and bissilole siloxane nanoaggregates in 90% water volume fraction were 32.4 % and 18.7%, respectively. The PL efficiencies for both nanoaggregates increased more than 40 times.

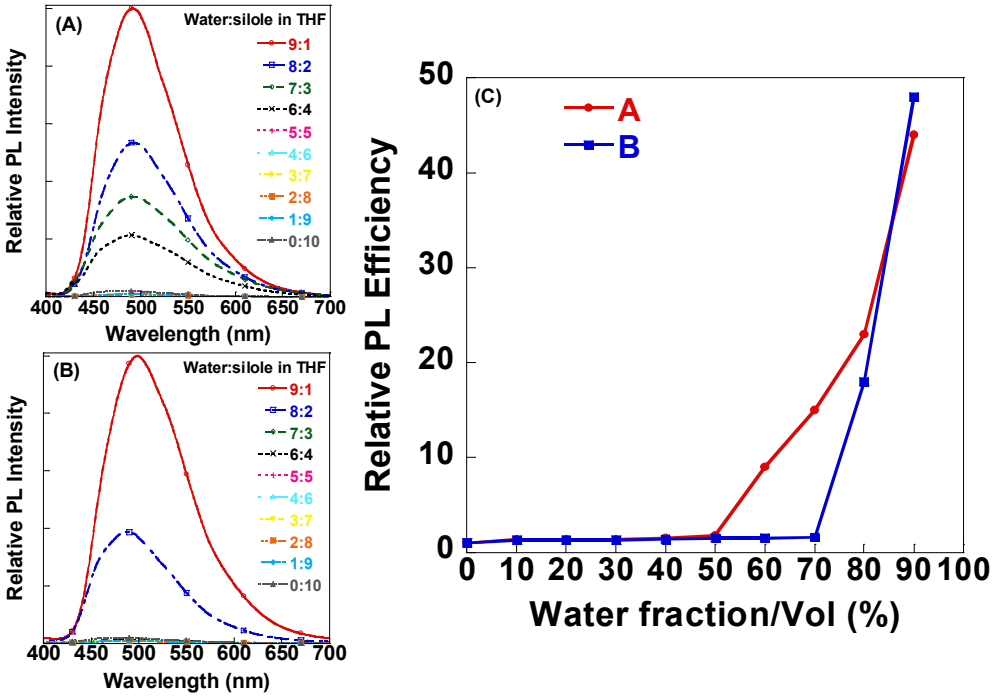

Figure 3.3 PL spectra of bis(methyltetraphenyl)silole (A) and bis(methyltetraphenyl)silole siloxane (B) nanoaggregates in water-THF mixtures (% water from top; 90%, 80%, 70%, 60%, 50%, 40%, 30%, 20%, 10%, 0%). Plot of the relative intensity of bis(methyltetraphenyl)silole nanoaggregate (red) and bis(methyltetraphenyl)silole siloxane nanoaggregate (blue) vs % water by volume (C).

Figure 3.3, obtained by dynamic light scattering measurements shows the size of nanoaggregate and size distribution in different water fractions. Particle diameter decreases as water fraction increases, but the dispersity of diameter for given any suspension is about ± 3%. Both nanoaggregates exhibit a minimum in size at 90% water. Average particle diameters for the bis(methyltetraphenyl)silole

nanoaggregate are 35, 60, 110, 260 nm as the water volume fraction decreases 90 to 60%, respectively. (See Figure 3.4A to 3.4D) Average particle diameters for the bis(methyltetraphenyl)silole siloxane nanoaggregate are 39 and 130 nm as the water volume fraction decreases 90 to 80%, respectively. (See Figure 3.4E to 3.4F) Decrease of particle size at higher water concentrations could be explained that the hydrophobic organic molecules are prone to aggregate to a higher extent in the hydrophilic environment.

The ability of the silole nanoaggregate with a volume-fraction of 90% water to detect TNT through PL quenching was investigated by adding successive aliquots of an identical volume-fraction of 90% water stock solution of TNT to the nanoaggregate. Figure 3.5A and 3.5B show quenching PL spectra of increasing fraction by 500 part per billion (ppb) of each TNT concentration in both silole nanoaggregates solution. The decrease in PL was monitored as a function of added TNT. The responses to quenching between both silole nanoaggregates were analyzed using the Stern-Volmer equation [22]: $I_0/I = K_{SV}[Q] + 1$. In this equation, I is the fluorescence intensity at quencher concentration, [Q], I_0 is the intensity at [Q] = 0, and K_{SV} is the Stern-Volmer constant. Linear Stern-Volmer relationships are observed for both nanoaggregates.

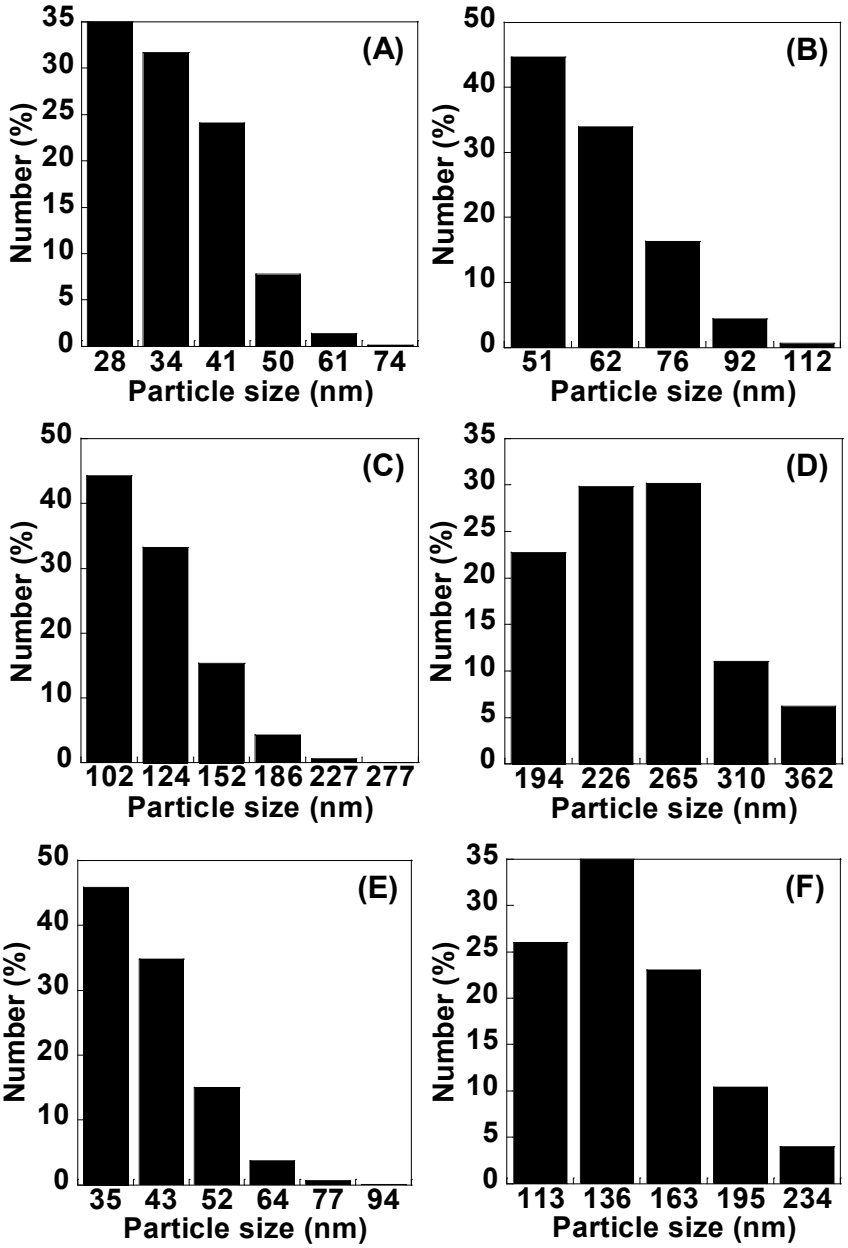

Figure 3.4 DLS data showing an increase in size when the water fraction ratio decreases to 90% (A), 80% (B), 70% (C), and 60% (D) for bis(methyltetraphenyl)silole nanoaggregate and 90% (E) and 80% (F)

for bis(methyltetraphenyl)silole siloxane nanoaggregate.

Stern-Volmer constant (K_{SV}) of bis(methyltetraphenyl)silole nanoaggregates and bis(methyltetraphenyl)silole siloxane nanoaggregates for TNT were 26,000 and 18,000 M^{-1}, respectively. Previously we reported that the Stern-Volmer constant of non-aggregate silole polymer, poly(tetraphenyl)siloles, for TNT detection was about 4,350 M^{-1} [14]. Trogler et al reported that the Stern-Volmer constant of oligo(tetraphenyl)silole nanoaggregate with a volume-fraction of 90% water was 4,100 M^{-1} [23]. Thus, the detection efficiency of bis(methyltetraphenyl)silole nanoaggregates in the water fraction of 90% for TNT increased by about 4 to 5 times compared to that of previous reported value. Higher detection efficiency of bis(methyltetraphenyl)silole nanoaggregates could be result from the conjugation through Si-Si bond between silole units.

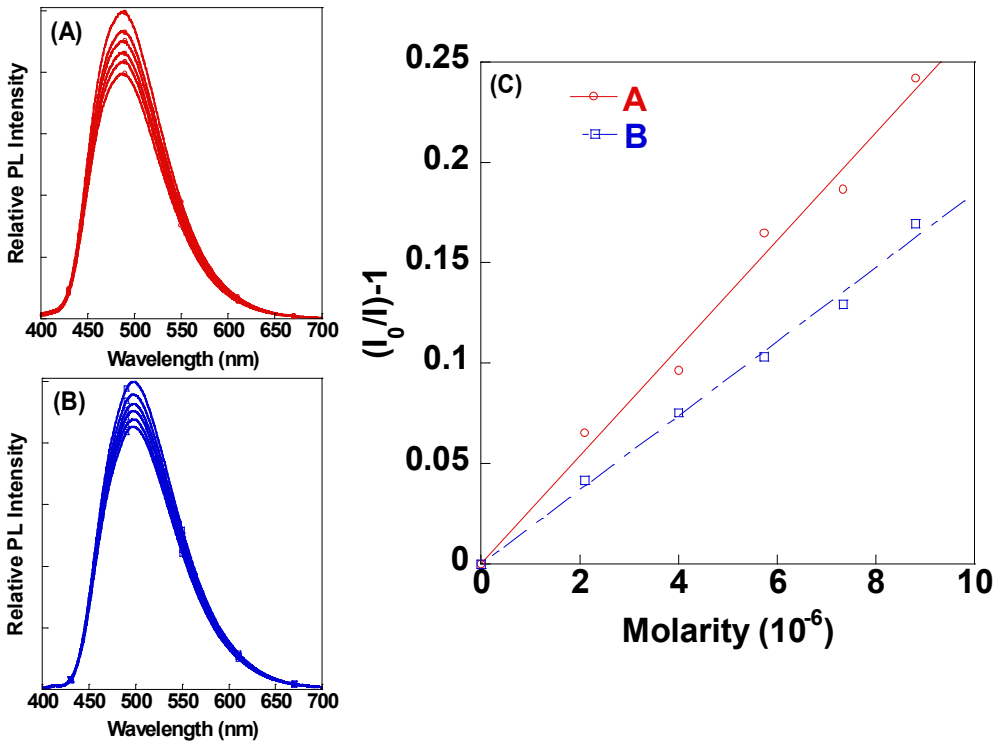

Figure 3.5 Quenching PL spectra of increasing fraction by 500 part per billion

(ppb) of each TNT concentration in bis(methyltetraphenyl)silole nanoaggregates solution (A) and bis(methyltetraphenyl)silole siloxane nanoaggregates solution (B). Stern-Volmer plot showing sensing efficiency for both nanoaggregates (C).

3.4 Conclusions

Aggregation-induced emission properties of conjugated silole nanoaggregates and non-conjugated silole siloxane nanoaggregates and their successful sensing of explosive were reported. Both silole nanoaggregates exhibited an aggregation-induced emission enhancement of more than 40 times increase to normal photoluminescence when the water fraction was increased to 90%. Both silole nanoaggregates used for the detection of TNT and showed greater sensitivity compared to previously reported value.

3.5 References

[1] G. M. Fischer, E. Daltrozzo, and A. Zumbusch, *Angew. Chem., Int. Ed.* 50, 1406 **(2011)**.

[2]. S. A. Jenekhe and J. A. Osaheni, *Science* 265, 765 **(1994)**.

[3]. Z. R. Grabowski and K. Rotkiewicz, *Chem. Rev.* 103, 3899 **(2003)**.

[4]. P. Bauer, H. Wietasch, S. M. Lindner, and M. Thelakkat, *Chem. Mater.* 19, 88 **(2007)**.

[5]. G. Sonmez, H. Meng, and F. Wudl, *Chem. Mater.* 15, 4923 **(2003)**.

[6]. J. Mei, Y. Hong, J. W. Y. Lam, A. Qin, Y. Tang, and B. Z. Tang, *Adv. Mat.* 26, 5429 **(2017)**.

[7]. R. West, H. Sohn, U. Bankwitz, J. Calabrese, Y. Apeloig, and T. Mueller, *J. Am. Chem. Soc.* 117, 11608 **(1995)**.

[8]. K. Tamao, M. Uchida, T. Izumizawa, K. Furukawa, and S. Yamaguchi, *J. Am. Chem. Soc*. 118, 11974 **(1996)**.

[9]. H. Sohn, R. R. Huddleston, D. R. Powell, and R. West, *J. Am. Chem. Soc*. 121, 2935 **(1999)**.

[10]. Y. Xu, T. Fujino, H. Naito, T. Dohmaru, K. Oka, H. Sohn, and R. West, *Jpn. J. Appl. Phys*. 38, 6915 **(1999)**.

[11]. Y. H. Park, Y. Kim, and H. Sohn, *J. Korean Phys. Soc.* 59, 2318 **(2011)**.

[12]. H. Sohn, R. M. Calhoun, M. J. Sailor, and W. C. Trogler, *Angew. Chem. Int. Ed.* 40, 2104 **(2001)**.

[13]. H. Sohn, M. J. Sailor, D. Magde, and W. C. Trogler, *J. Am. Chem. Soc.* 125, 3821 **(2003)**.

[14]. J.-K. Choi, S. Jang, K.-J. Kim, H. Sohn, and H.-D. Jeong, *J. Am Chem. Soc*. 133, 7764 **(2011)**.

[15]. J. Luo, Z. Xie, J. W. Y. Lam, L. Cheng, H. Chen, C. Qiu, H. S. Kwok, X. Zhan, Y. Liu, D. Zhu, and B. Z. Tang, *Chem. Commun*.1740 **(2001)**.

[16]. S. Jang, S. G. Kim, D. Jung, H. Kwon, J. Song, S. Cho, Y. C. Ko, and H. Sohn, *B. Kor. Chem. Soc*. 27, 1965 **(2006)**.

[17]. L. C. Palilis, A. J. Maekinen, M. Uchida, and Z. H. Kafafi, *Appl. Phys. Lett.* 14, 2209 **(2003)**.

[18]. L. C. Palilis, A. J. Maekinen, M. Uchida, and Z. H. Kafafi, *Appl. Phys. Lett*. 14, 2209 **(2003)**.

[19]. M. H. Lee, D. Kim, Y. Dong, and B. Z. Tang, *J. Korean Phys. Soc.* 45, 329 **(2004)**.

[20]. A. Sekiguchi, S. S. Zigler, and R. West. *J. Am. Chem. Soc*. 108, 4241-4242 **(1986)**.

[21]. N. J. Turro, Modern Molecular Photochemistry, University Science Books, Sausalito, California **(1991)**.

[22]. S. J. Toal, D. Magde, and W. C. Trogler, *Chem. Commun.* 5465 **(2005)**.

[23]. I. Toulokhonova, R. Zhao, M. Kozee, and R. West, *Main Group Metal Chemistry* 24, 737-774 **(2011)**.